A Deterministic Model for Contact Surfaces at Dielectric Interfaces Subjected to an Electrical Field

Emre Kantar[†§]
[†]Department of Electric Power Engineering, Norwegian University of Science and Technology, Trondheim, Norway
[§]Department of Electric Power Technology, SINTEF Energy Research, Trondheim, Norway

***Abstract*—This paper presents theoretical and experimental studies aiming to explore the effects of the elastic modulus and surface roughness on tangential AC breakdown strength (BDS) of interfaces between polymers. Four different polymers with different elastic moduli were tested. The interfaces were formed between identical specimens and were AC breakdown tested at various contact pressures. In addition, interface surfaces were polished using four different sandpapers of different grit sizes to study the effect of surface roughness. A deterministic model based on the tribology of solid surfaces was proposed to simulate the deformation of the surface asperities in 3D as a function of the contact pressure, surface roughness, elastic modulus, and hardness of an interface. The simulation results were correlated with the results of the AC breakdown experiments, and they elucidated how cavities were linked at solid-solid interfaces and enabled the estimation of the gas pressure inside the cavities under different circumstances (roughness, elasticity, and pressure).**

I. Introduction

The series connection of dielectric materials constitutes the electrical insulation system in most high-voltage (HV) equipment and accessories. The alternating current (AC) breakdown strength (BDS) of insulation systems is limited by the lowest BDS of either the bulk insulating materials or the interface between adjacent insulating materials. When two nominally flat surfaces make contact, the actual surface is not perfectly smooth, and the actual contact at the interface is also not ideal, leading to numerous microcavities (used interchangeably with cavity) between adjacent contact spots [1], [2].

Cavities are likely to cause partial discharges (PD) and trigger interfacial tracking that can eventually lead to a premature electrical breakdown (BD) [3], [4]. In addition, the dielectric medium inside the cavities influences the PD inception field strength [5], [6]. An interface, thus, is a weak point likely to reduce the tangential AC BDS of an HV insulation system due to local electric field enhancements in the cavities [3]–[5], [7].

Scholars have mainly investigated the characteristics of insulation materials, such as the bulk BDS, surface flashover, surface tracking, and erosion without scrutinizing the solid-solid interfaces separately. Few studies have focused on the interfacial HV insulation performance between two solid dielectrics [3], [4], [7]. It was reported that the elasticity and surface roughness of the solid materials, dielectric medium surrounding the interfaces, and interfacial pressure are important factors affecting the dielectric strength of an interface. Also, the author's previous studies, concerning the tangential AC BDS of solid interfaces [6], [8], [9], demonstrated significant dependencies on these factors. However, neither the mechanisms governing the interfacial BD nor the correlation between the shape/size, number of cavities (size of contact area) and the interfacial BD has yet been fully understood.

Kato et al. [7] examined the correlation between the pressure distribution and the interfacial AC BD voltage. Though their experimental results were in line with the above-mentioned literature, they highlighted the need for realistic modeling of the deformation of microcavities between two solid dielectrics to further explain the correlation between the interfacial morphology and the interfacial BDS. The author's previous work also demonstrated the need for an intricate 3D interface contact model. To that end, in this paper, the interfacial morphology under different contact pressures, roughnesses, and elastic moduli were studied using both theoretical modeling and experimental verification. A novel deterministic model based on the tribology of solid materials was proposed to simulate the deformation of the surface asperities in 3D as a function of the contact pressure, surface roughness, elastic modulus, and hardness of an interface. Using the model, the densities of the cavities and the real contact area under different levels of roughnesses, elasticities, and interface pressures were analyzed. Next, tangential AC interfacial BD experiments under different interface pressures, roughness levels, and elasticities were conducted. Finally, the correlation between the interfacial AC BDS and interface morphology was analyzed.

II. Experimental Procedure

To test the tangential AC BDS of solid-solid interfaces as a function of elasticity, we assembled four different interfaces at dry conditions using four different materials with different elastic moduli. The interfaces were formed between the same materials: cross-linked polyethylene (XLPE), epoxy, polyether ether ketone (PEEK), and silicone rubber (SiR) under various contact pressures applied by means of different mechanical loads (XLPE–XLPE, PEEK–PEEK, and so on). Alternatively, elastic modulus could be varied by adding micro- and nano-scaled particles such as zinc oxide, zirconia, and silica, yet, adding such fillers causes as significant a change in the chemical/electrical properties as does selecting a different polymer [9]. The relative permittivities of SiR, XLPE, EPOXY, and PEEK are 2.8, 2.3, 4.6, and 2.8, respectively. The samples were cut/molded in rectangular prisms ($4\,\mathrm{mm} \times 55\,\mathrm{mm} \times 30\,\mathrm{mm}$), and two samples were positioned vertically on top of each other between two Rogowski-shaped electrodes forming a 4-mm-long interface, as illustrated in Fig. 1.

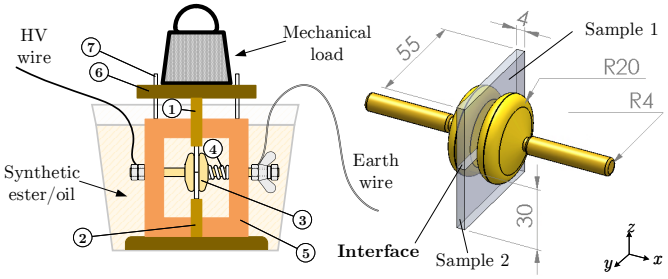

Fig. 1: Mechanical test setup used in the AC breakdown experiments: (1) Movable (upper) pressure transfer block. (2) Fixed (lower) interface pressure keeper block. (3) Rogowski-shaped electrodes. (4) Helical spring. (5) Supporting frame. (6) Epoxy plate. (7) Weight stabilizing epoxy bars. Dimensions are given in mm. Details of the setup can be found in [5].

The contact surfaces of the samples were polished using a table-top, grinding machine. We fixed the specimens in a steel rotating disk and positioned round-SiC sandpaper on the rotating plate [8]. To study the effect of surface roughness on the tangential AC interfacial BDS, we used XLPE samples of four different surface roughnesses. Contact surfaces were polished using sandpapers of grit #180 (roughest), #500, #1000, or #2400 (smoothest). In the elastic modulus experiments, all samples were polished using #500.

A 50-Hz AC ramp voltage at the rate of $1\,\mathrm{kV/s}$ was applied until breakdown. All breakdown tests were performed with the setup immersed in oil (synthetic ester–Midel 7131) to prevent any external flashover. To avoid penetration of oil into the interface, we applied the load before filling the test chamber with the oil. Desired contact pressure was exerted using weights varying between $3-75$ kg ($0.16-3.34\,\mathrm{MPa}$) to press the samples vertically against one another, as illustrated in Fig. 1. The average contact pressure was then calculated using the nominal contact area of $A_a = 4\,\mathrm{mm} \times 55\,\mathrm{mm} = 220\,\mathrm{mm}^2$. The applied pressure levels were determined via preliminary tests, where the samples and the interface were checked against deformation and oil penetration. For instance, testing of the XLPE–XLPE interface was not viable above $1.67\,\mathrm{MPa}$ due to the physical deformation of the samples. Likewise, the SiR samples start to deform at contact pressures beyond $0.27\,\mathrm{MPa}$, rendering testing at higher contact pressures not possible due to the likelihood of oil penetration. Oil-mate interfaces had also been tested to verify the reliability of the setup in preventing undesired oil penetration within the determined contact pressure range for each interface [6].

For each interface at each contact pressure and surface roughness, eight measurements were performed using an unused pair of samples for each of eight repetitions. The results were statistically assessed using the two-parameter Weibull distribution. The nominal value of the Weibull (63.2%) with the 90% confidence intervals (CI) were used. Goodness-of-fit, in each case, was tested following the guidelines in [10]. To obtain the real 3D surface data for the model, we characterized the morphology of the polished sample surfaces using a 3D-optical profilometer (Bruker ContourGT-K). 50X magnification with $0.2\,\mu\mathrm{m}$ lateral and $3\,\mathrm{nm}$ vertical sampling resolution was chosen to scan a surface area of $1.25\,\mathrm{mm} \times 0.94\,\mathrm{mm}$, whose data was stored in a 480×640 matrix.

III. Deterministic Contact Model for Asperities at Solid-Solid Interfaces

The primary motivation for developing the deterministic model is to simulate the deformation of the surface asperities in 3D as a function of the contact pressure, surface roughness, elasticity, and hardness of insulation material. The model elucidates how cavities are connected at solid-solid interfaces in components and enables estimation of the gas pressure inside the cavities. The model is based on the equivalent rough surface model, as illustrated in Fig. 2 and incorporates linear elastic and perfectly plastic contacts [1]. Owing to the model, 3D in-contact topography and the respective pressure distribution at the contact spots are acquired.

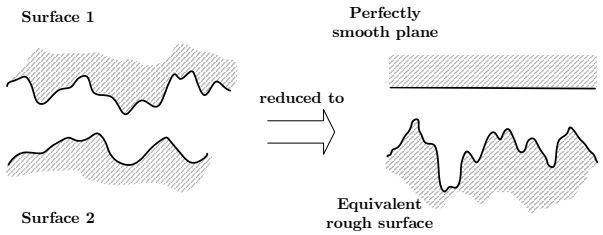

Fig. 2: Contact asperities between a perfectly smooth surface and a rough surface. Greenwood and Tripp [1] showed that the contact of two rough surfaces could be reduced to a so-called equivalent sum surface, consisting of a single, rough surface with a smooth, rigid plane. For details, refer to Chapter 3 in [5].

The contact between real-life topographies leads to plastic deformations at the contact spots, even under relatively small loads [5]. Tian and Bhushan [11] built their theoretical model on a variational principle for both linear elastic and linear elastic-perfectly plastic materials, where the plastic deformation of contact spots is covered for real contact surfaces. In the variational method, the real area of contact and contact pressure distributions are the variables, which minimize the total complementary potential energy [2], [11]. In this work, the upgraded model by Almqvist [12] based on the Tian and Bhushan's model [11] is used to account for the energy dissipation due to plastic deformations.

Assuming frictionless linear elastic contact, total complementary potential energy (the variational problem allowing 2D and 3D topographies) is given by [12]:

$$\min_{0\le p_a\le H_s}(F) = \min_{0\le p_a\le H_s}\left(\frac{1}{2}\int_\Omega p_a\,\delta_e\,d\Omega - \int_\Omega p_a\,((h_2-h_1)-\delta_p)\,d\Omega\right), \tag{1}$$

$$\int_\Omega p_a\,d\Omega = W_m\,, \tag{2}$$

where Ω is an arbitrary area, H_s is the hardness of the softer material (in the case of two different materials forming an interface), p_a is the contact pressure, $\delta_e = z - d$ is the elastic deformation with reference to Fig. 3, $h_g = h_2 - h_1$ is the gap between the undeformed surfaces, δ_p is the amount of plastic deformation, and W_m is the applied load. Equation (1) is limited by two main constraints such that the maximum

pressure is limited to the hardness of the softer material, i.e., $p_a \leq H_s$, while it is assumed equal to or greater than zero. In this way, the local contact pressure increases with increasing normal load for elastic contact spots, resulting in larger real contact area [12].

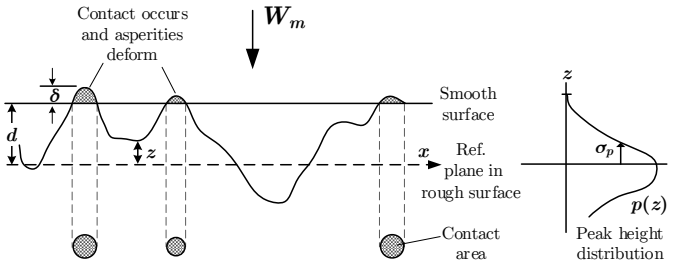

Fig. 3: Schematic representation of the contact between a rough surface and a smooth surface (rigid plane) [2].

For two elastic half-spaces, the amount of deflection of elastic surface $\delta_e(x)$ at a given pressure is expressed as [12]:

$$\delta_e(x) = -\frac{4}{\pi E'} \int_{-\infty}^{\infty} \ln|x-s|\, p_a(s)\, ds + C\,, \qquad (3)$$

where C is an arbitrary integral constant. The elastic modulus of an interface E', i.e. the effective modulus, is calculated using the individual elastic modulus of each material forming the interface, as shown in [9]. Measured elasticities of the materials and the elasticity of sum surfaces used in this work are available in [5], [9] (also shown in Fig. 5).

To sum up, the contact problem of finding a minimum value of the total complementary potential energy is reduced to solving the minimum value problem of the integral in (1) in terms of contact pressure. Readers may refer to Chapter 5 in [5] for the details on the discretization of surface profiles, solution techniques, and implementation of the algorithm.

The outputs of the deterministic model will be displayed using contour plots. Contour lines are extracted from the intersection of the surfaces with horizontal planes at different heights, as illustrated in Fig. 4(a). An array of contour lines is generated by shifting the plane to evenly spaced height levels, as illustrated in Fig. 4(b). Contour lines in this work represent the amplitudes of the asperities as well as the area of cavities and contact spots at a solid-solid interface. Different levels are represented by different colors, where red indicates the highest peak, and light yellow indicates the zero level.

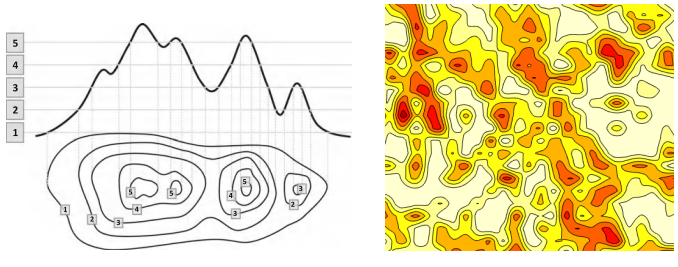

(a) (b)

Fig. 4: (a) Contour lines representing the surfaces with planes at different amplitudes [13]. (b) Filled-contour lines colored based on height/amplitude.

IV. Results

A. AC Breakdown Experiments

The effect of the elastic modulus on the tangential AC BDS of solid-solid interfaces between the same polymers, SiR, XLPE, EPOXY, and PEEK, was tested at various interfacial contact pressures with all the samples polished using the same sandpaper #500. The nominal 63.2% values for each interface are shown in Fig. 5 with corresponding 90% CI values. Breakdowns always occurred along the interface in all the experiments owing to the designed test setup. Results demonstrated that the increased elastic modulus resulted in a reduced BDS. The effect of the contact pressure was also discernible such that increased contact pressure by a factor around 3 increased the interfacial BDS by a factor of 1.4 in the case of the lowest elastic modulus (SiR–SiR), whereas the BDS value in the case of highest modulus (PEEK–PEEK) became 2.4-fold. It was observed that materials with relatively low moduli such as SiR and XLPE yielded higher interfacial BDS values even at relatively low contact pressures.

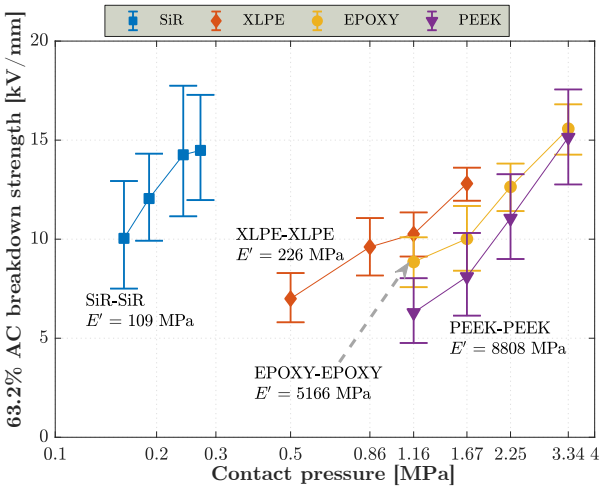

Fig. 5: Results of the tangential AC breakdown experiments vs. the contact pressure at which interfaces between the identical materials (sanded using #500 grit) were tested. The markers stand for 63.2% BDS while error bars represent 90% CI of the 63.2% values.

Effect of the surface roughness on the interfacial BDS was investigated at 0.5, 0.86, and 1.16 MPa contact pressures. Similarly, only 63.2% values with 90% CI are plotted against the sandpaper grit in Fig. 6, while each bar graph represents the arithmetic mean height S_a of the asperities (calculated using the real 3D surface data) at each interface. Results indicated that the interfacial BDS reduced as the surface roughness was increased, whereas higher contact pressure led to an increased BDS. The 63.2% BDS in the case of the surface polished by #2400 was nearly twice as high as that in the case of #180 at each contact pressure.

B. Deterministic Roughness Model

It is important to recollect that an interface between two rough surfaces was transformed into an interface between one perfectly smooth plane and one equivalent rough surface (sum surface of the roughnesses of both surfaces), as illustrated in the 3D Cartesian coordinates in Fig. 7. Moreover, the 3D

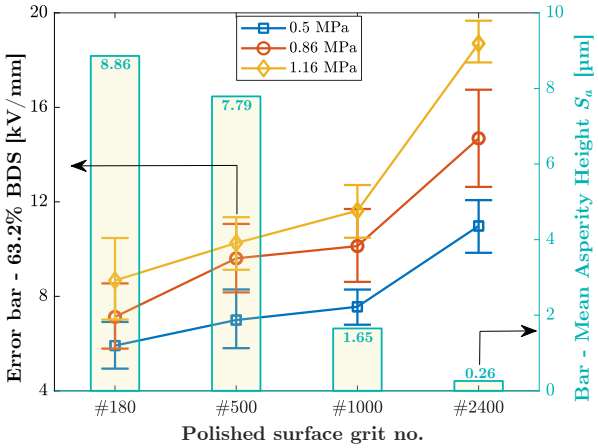

Fig. 6: (i) Left y-axis: Experimental results of tangential AC BDS of interfaces vs. the polished rough surface grit no. of XLPE samples. (ii) Right y-axis: Arithmetic mean asperity height S_a shown by the bars.

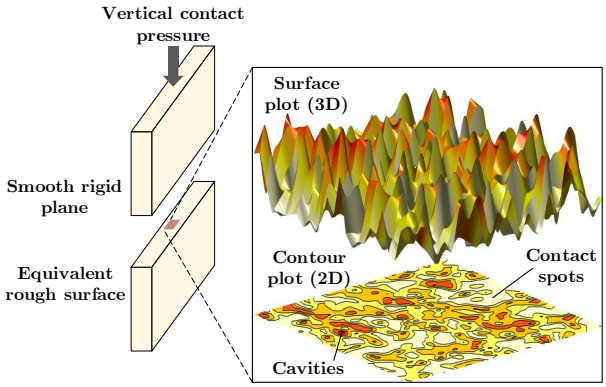

Fig. 7: Contact asperities between a perfectly smooth surface and a rough surface. Red color represents the highest peak, and light yellow/white represents the contact points.

surface topography was mapped on a 2D plane using contour lines with color bars displaying the amplitudes of the peaks quantitatively (see Fig. 8). Simulation results were run at two different contact pressures—the lowest and highest pressure values at which the samples were tested in the AC breakdown experiments (see Fig. 5). An exception was made in the case of XLPE by setting the highest pressure to the next higher level to simulate to what further extent cavities shrink, and hence the contact area increases.

1) Effect of Surface Roughness and Contact Pressure: Fig. 8 shows contour plots of the surface asperities of the XLPE samples of four different surface roughnesses. The contour plots suggest that increased pressure pushes the asperity tips further, leading to the formation of new contact spots. As a result, more cavities are formed due to channels (large air vents) being broken into smaller channels and cavities. Towards smoother interfaces, the density of the peaks reduces considerably, and the impact of the increased pressure becomes even more discernible. Particularly in the case of XLPE #2400, there were only a few protruding peaks at the surface, while the rest of the surface seemed to be perfectly smooth.

2) Effect of Elastic Modulus and Contact Pressure: To present the effect of elasticity and contact pressure, the simulated deformation and displacement of the asperities of

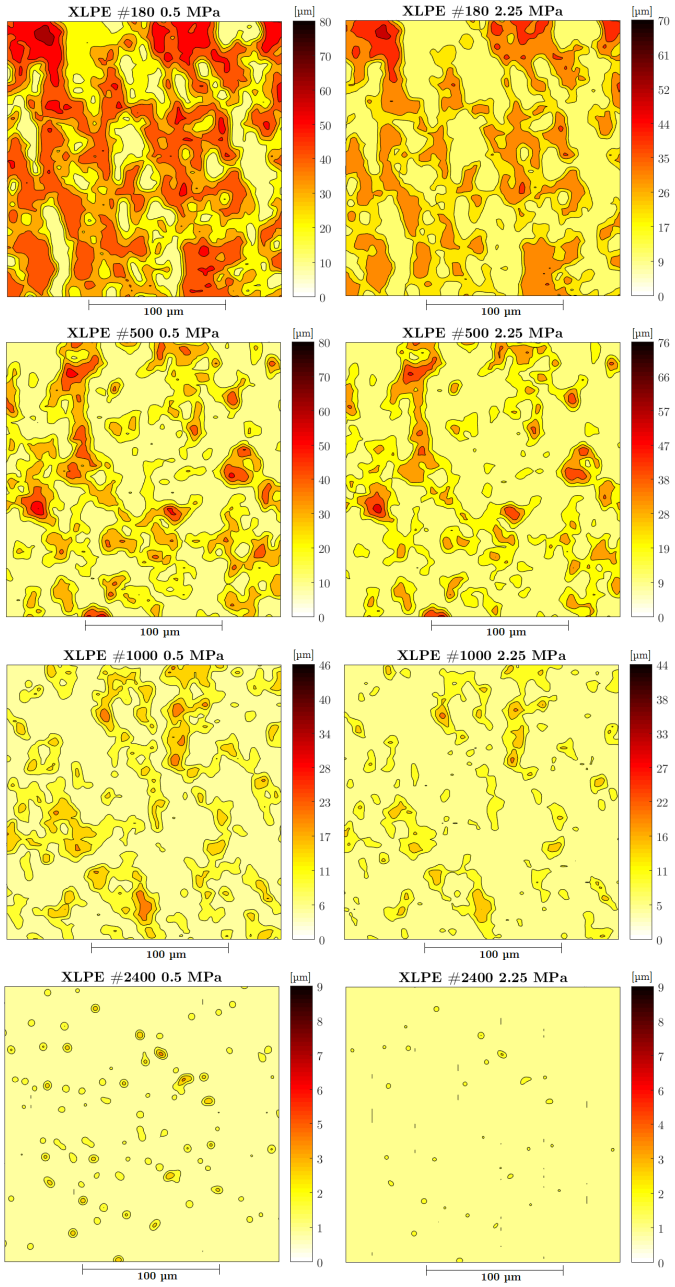

Fig. 8: Filled-contour plots of the surface asperities of the XLPE samples polished with #180, #500, #1000 and #2400 at 0.5 MPa (lowest p_a) and 2.25 MPa (highest p_a), respectively. Color bars are in µm, where light yellow color represents the contact areas, and darker colors indicate cavities.

the XLPE and PEEK samples in 2D are shown in Fig. 9. The waveforms represent equivalent rough surfaces while the horizontal axes stand for perfectly smooth planes (no asperities hypothetically, as illustrated in Fig. 2). Thus, the areas between the adjacent contact spots are the cavities formed between the surfaces. The widths of cavities in the PEEK samples in the direction of the tangential electrical field were larger than those of the XLPE samples despite having been sanded by the same #500-grit sandpaper. To improve readability, a smaller section of the interface of XLPE is shown, i.e., 0.3 mm. Consequently, higher pressure pushes the asperity tips

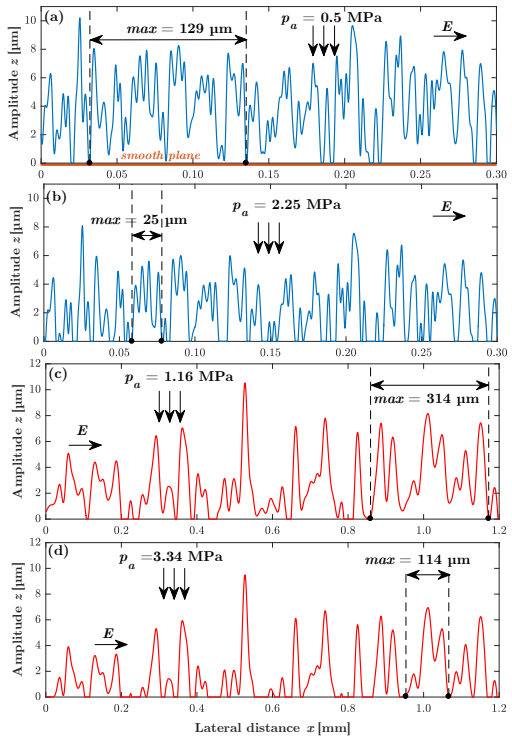

Fig. 9: The displacement of peaks at the interface: (a) XLPE-XLPE #500 at 0.5 MPa. (b) XLPE-XLPE #500 at 2.25 MPa. (c) PEEK-PEEK #500 at 1.16 MPa. (d) PEEK-PEEK #500 at 3.34 MPa. E shows the direction of the tangential field component.

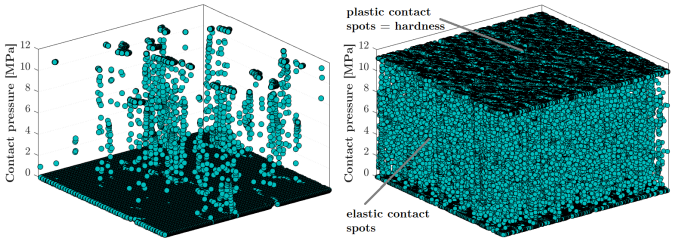

(a) Elastic contacts, few plastic contacts. (b) Elasto-plastic contacts

Fig. 10: Pressure distribution at contact spots. Each spherical marker represents the contact pressure at the shown position.

forward, leading to the formation of new contact spots. As a result, large cavities/channels break into smaller cavities. The deformation of the asperity tips can be envisaged in such a way that the perfectly smooth rigid plane (horizontal axis) is pressed against the equivalent rough surface as more of the afloat asperities come into contact with the smooth surface, resulting in more contact spots, and hence smaller cavities. Note that these profiles constitute a small portion of the complete surface data, as illustrated with the red rectangle in Fig. 7. The complete surface data set was excessively large to be demonstrated in a single graph. The unrevealed parts of the surfaces had similar, uniform patterns.

Pressure distributions at the contact surfaces of the XLPE #500 and PEEK #500 samples at 1.16 MPa are shown in 3D in Fig. 10. Each spherical marker in Fig. 10 represents the contact pressure at the shown position at the surface. If the contact is elastic, the contact pressure ranges between zero and the hardness of the material, as illustrated in Fig. 10(a). On the other hand, once the hardness of the material is reached, elastic contact spots transition to plastic contacts, and the contact area does not increase any more even if the applied force is further increased. Thus, at plastic contact spots, the max. pressure is limited by the hardness of the material, as illustrated in Fig. 10(b). In this regard, the deformation of contact asperities was significantly lower in the case of PEEK (hard) even at higher contact pressures than in the case of XLPE (soft).

V. Discussion

The interface simulations indicated that the increased interfacial pressure reduced the number of long, vented air-gaps and thus created more enclosed cavities at the interface. Likewise, the smoother the surface was, the more enclosed, smaller cavities were present. Conversely, harder interfaces brought about larger cavities, that in turn, resulted in long channels due to interconnected cavities. These findings suggest that increased contact pressure, increased elastic modulus (harder materials), and/or decreased surface roughness generate smaller cavities. Consequently, vented channels and enclosed cavities at the interface are likely to coexist, especially in the cases of moderate roughnesses, contact pressures, and material elasticities. The state of the coexistence of vented and enclosed cavities can be deemed as a transition from soft, smooth interfaces at high contact pressure to hard, rough interfaces at low pressure.

Figs. 11(a) and (c) illustrate the case when only enclosed cavities are present at an interface such as in the cases of soft materials, high contact pressure, and/or smooth surfaces. Conversely, Figs. 11(b) and (d) demonstrate that, nearly, only vented channels exist at the interfaces, as in the cases of hard materials, rough surfaces, and/or low contact pressure. Possible surface paths, likely to be tracked in the event of an interface breakdown, are illustrated in Figs. 11(a)–(b) for each case. In the case of "only enclosed cavities," contact spots must be subjected to an electrical breakdown in addition to the discharge of cavities. On the other hand, in the case when air-filled, interconnected cavities are prevalent at the interface, an interface tracking path can be formed by incorporating only the vented air-gaps, as illustrated in Fig. 11(b).

In particular, as presented in Fig. 8, the increased contact pressure in the case of the smoothest interface, XLPE #2400, led to an almost perfect/ideal contact between the XLPE samples. In conjunction with the larger contact area that the simulations suggested, very high AC BDSs were measured in the case of XLPE #2400, particularly at higher contact pressures, as shown in Fig. 6. In addition, the increased contact pressure from 0.5 to 1.16 MPa in the case of XLPE #180 yielded a higher BDS by a factor of 1.4, while it was 1.7 in the case of #2400 (see Fig. 6). These results indicate that the smoother the surface is, the higher the influence of the increased pressure is on the measured BDS. To sum up, the gas pressure inside an isolated cavity is likely to increase as a function of the change in the cavity sizes (the extent of which is dependent on the contact pressure and elastic modulus), which in turn, increases the discharge field strength of the cavities according to the right-side of the Paschen minimum. Consequently, the increased gas pressure inside

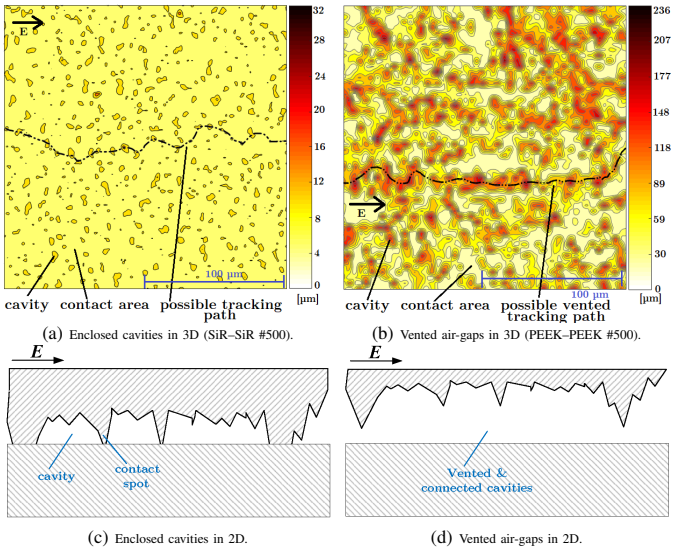

(a) Enclosed cavities in 3D (SiR–SiR #500).

(b) Vented air-gaps in 3D (PEEK–PEEK #500).

(c) Enclosed cavities in 2D.

(d) Vented air-gaps in 2D.

Fig. 11: Simulated interfacial surfaces incorporating only enclosed cavities and vented air-gaps formed by interconnected cavities.

isolated/enclosed cavities was likely to have contributed to the very high BDS values achieved at smoother interfaces at high contact pressures in the AC breakdown experiments. A similar claim can be made for softer materials (lower elastic modulus) such as SiR. The very high AC BDS values of SiR–SiR #500 displayed in Fig. 5 suggest that there were probably numerous enclosed cavities even at a relatively low contact pressure, inside of which the gas pressure was greater than $1\,\mathrm{atm}$. Fig. 11(a) indicates that there were many enclosed cavities even at very low pressure ($0.16\,\mathrm{MPa}$) at the SiR–SiR #500 interface, which were broken into even smaller cavities at a slightly higher contact pressure. Likewise, despite the significant difference in elasticity, at high contact pressures, the coexistence of vented air-gaps and enclosed cavities was very likely to be the case regarding the elevated AC BDS values measured in the cases of XLPE #500, EPOXY #500, and PEEK #500. These findings agree with the reported results by Stewart et al. [14] that vented channels are likely to be subjected to less severe PDs due to the dispersal of by-products and gas refresh through the vents. This is because the variation in the gas content and by-products generated by the PDs in the cavities affect the space charge build-up on the cavity walls, the generation rate of initiating electrons, and alter the collision energy; thus changing the PD features [14]. Also, Kato et al. [7] reported that streamer propagation was suppressed at a high-pressure region at the interface (supporting the presence of enclosed gaps), which led to a higher AC BD voltage, while the lowest AC BD voltage was measured in the case of the hardest interface.

VI. Conclusion

In this paper, the correlation between the tangential AC BDS of solid-solid interfaces and the interface morphology was studied theoretically and experimentally. A novel deterministic interface model based on the tribology of solid materials was proposed to simulate the deformation of the surface asperities in 3D as a function of the contact pressure, surface roughness, elastic modulus, and hardness of an interface. The deterministic interface model indicated that increased contact pressure reduced the number of long, vented air-gaps, and thus, created more enclosed cavities at an interface. Likewise, the smoother the interface was, the more enclosed, smaller cavities were present. Conversely, harder interfaces brought about larger cavities; thus, long vented air-gaps were formed by the interconnected cavities: vented and enclosed cavities at an interface are likely to coexist in real life. Hence, the gas pressure inside the enclosed cavities is likely to increase as a function of the change in the cavity sizes, the extent of which is dependent on the contact pressure and elastic modulus.

The results of the AC breakdown experiments indicated that interface pressure, roughness, and elastic modulus significantly affected the BDS of solid-solid interfaces. The interfacial BDS values in the cases of softer interfaces, SiR–SiR and XLPE–XLPE, were found to be higher than those of the harder interfaces, EPOXY–EPOXY and PEEK–PEEK. Likewise, smoother interfaces and higher contact pressures led to considerably higher AC BDS values. To conclude, the experimental findings were in good agreement with the simulation results: under the conditions when the model suggested the prevalence of enclosed cavities (or vented air-gaps), the AC BDS values were found to be relatively high (or low).

References

[1] J. Greenwood and J. Tripp, "The contact of two nominally flat rough surfaces," *Proc. Instit. Mech. Eng.*, vol. 185, no. 1, pp. 625–633, 1970.

[2] B. Bhushan, "Contact mechanics of rough surfaces in tribology: multiple asperity contact," *Tribology Letters*, vol. 4, no. 1, pp. 1–35, 1998.

[3] B. Zhu, Z. Jia, H. Hu, X. Ouyang, and X. Wang, "Relationship between the Interfacial Ramped DC Breakdown Voltage and the Morphology of the XLPE/SiR Interface," *IEEE Trans. Dielectr. Electr. Insul.*, vol. 26, no. 3, pp. 689–697, Jun. 2019.

[4] B. Du, X. Zhu, L. Gu, and H. Liu, "Effect of surface smoothness on tracking mechanism in XLPE-Si-rubber interfaces," *IEEE Trans. Dielectr. Electr. Insul.*, vol. 18, no. 1, pp. 176–181, 2011.

[5] E. Kantar, "Longitudinal AC Electrical Breakdown Strength of Polymer Interfaces," Ph.D. dissertation, Norwegian Uni. Sci. Tech., 2019.

[6] E. Kantar, D. Panagiotopoulos, and E. Ildstad, "Factors Influencing the Tangential AC Breakdown Strength of Solid-Solid Interfaces," *IEEE Trans. Dielectr. Electr. Insul.*, vol. 23, no. 3, pp. 1778–1788, 2016.

[7] M. Kato, Y. Nishimura, N. Osawa, Y. Yoshioka, H. Yanase, and K. Okamoto, "Effects of Compressive Force and Dielectric Materials on Contact Area for High-Pressure Region and Interfacial AC Breakdown Between Two Solid Dielectrics," in *Proc. 21st Int. Symp. HV Eng. (ISH 2019)*. Springer Int., 2020, pp. 118–129.

[8] E. Kantar, S. Hvidsten, F. Mauseth, and E. Ildstad, "Longitudinal AC Breakdown Voltage of XLPE-XLPE Interfaces Considering Surface Roughness and Pressure," *IEEE Trans. Dielectr. Electr. Insul.*, vol. 24, no. 5, pp. 3047–3054, 2017.

[9] E. Kantar, S. Hvidsten, and E. Ildstad, "Effect of Material Elasticity on the Longitudinal AC Breakdown Strength of Solid-Solid Interfaces," *IEEE Trans. Dielectr. Electr. Insul.*, vol. 26, no. 2, pp. 655–663, 2019.

[10] IEC 62539 First Edition 2007-07 IEEE 930, "IEC/IEEE Guide for the Statistical Analysis of Electrical Insulation Breakdown Data (Adoption of IEEE Std 930-2004)," pp. 1–53, 2007.

[11] B. Bhushan and X. Tian, "A numerical three-dimensional model for the contact of rough surfaces by variational principle," *ASME J. Tribol*, vol. 118, pp. 33–42, 1996.

[12] A. Almqvist, "On the effects of surface roughness in lubrication," Ph.D. dissertation, Luleå tekniska universitet, 2006.

[13] R. Leach, *Characterisation of areal surface texture*. Springer, 2013.

[14] D. Adhikari, D. M. Hepburn, and B. G. Stewart, "PD characteristics and degradation in PET insulation with vented and unvented internal voids," *Electr. Power Systems Research*, vol. 100, pp. 65–72, Jul. 2013.